Supplementary Material for:

Phytoplankton community succession and biogeochemistry in a mesocosm bloom simulation at an estuary-ocean interface

Jenna A. Lee[1], Joseph H. Vineis[1,§], Mathieu A. Poupon[1,2], Laure Resplandy[1,3], Bess B. Ward[1,3]

[1]Department of Geosciences, Princeton University, Princeton, NJ, 08544, USA
[2]Atmospheric and Oceanic Sciences Program, Princeton University, Princeton, NJ, 08544, USA
[3]High Meadows Environmental Institute, Princeton University, Princeton, NJ, 08544, USA
[§]*Current affiliation*: Marine Biological Laboratory, University of Chicago, Woods Hole, MA, 02543, USA

Correspondence to: Jenna A. Lee (jennaal@princeton.edu)

1 Methodology

1.1 Mesocosm Design and Sampling Protocols

Incubation medium was prepared by pumping surface water (~5 m) directly from the sample site through a series of polycarbonate (PC) mesh filters (~300 μm, 20 μm, and 5 μm) followed by 0.7 μm and 0.3 μm glass fiber filters using a double diaphragm pump. All materials used to set up and sample the mesocosms were soaked in 1 M HCl overnight and rinsed 3 times with MilliQ water. Additionally, all sampling materials and sub–incubation bottles were acid– and MilliQ–rinsed between sampling events and rinsed twice with sample water prior to sample collection unless otherwise stated. Before subsampling, each carboy was gently mixed by rolling on its side. Water was collected for samples into carboy–specific PC bottles and aliquoted for the various sample types using graduated cylinders.

50 mL conical tubes for nutrient samples were rinsed twice with MilliQ water before sample collection. Duplicate nutrient samples were taken when possible. Nutrient samples were then frozen upright and stored at -20º C until in–lab analysis.

Sample water for pigment samples and ^{5}N–NO$_3^-$ and ^{13}C–HCO$_3^-$ sub–incubations was aliquoted using an acid–cleaned graduated cylinder. Water for pigment samples was kept in the dark at ambient temperatures until it could be filtered. All filters were folded in half, topside in, and stored individually in glassine envelopes. Sub–incubation samples were separated by label and stored at -20º C. Pigment samples were additionally wrapped with aluminum foil and stored at -80º C until being shipped to the Baruch Institute for Marine and Coastal Sciences at the University of South Carolina for analysis.

1.2 Nutrient–Phytoplankton–Zooplankton (NPZ) Model

We use a plankton ecosystem model to assess the potential impact of zooplankton grazing on phytoplankton accumulation
during the three experiments. This model is a simplified version of the biogeochemical model Carbon, Ocean Biogeochemistry
and Lower Trophics version 2 (COBALTv2, (Stock et al., 2020) and represents the dynamics of nitrogen within five pools:
nitrate (N_{NO3}), phytoplankton (N_{Phyto}), zooplankton (N_{Zoo}), detritus ($N_{Detritus}$) and dissolved organic matter (N_{DOM}). The
model is used to evaluate the temporal evolution of the different pools assuming no spatial variations (i.e. zero–D, only time
dependent). Nitrogen is transferred from one pool to another via biogeochemical fluxes (e.g.
$growth, remineralization, respiration, grazing$):

$$\frac{dN_{NO3}}{dt} = respiration + remineralization_{DOM} + remineralization_{Detritus} - growth_{Phyto} \qquad (S1)$$

$$\frac{dN_{Phyto}}{dt} = growth_{Phyto} - grazing \qquad (S2)$$

$$\frac{dN_{Zoo}}{dt} = \varepsilon\, grazing - mortality - respiration \qquad (S3)$$

$$\frac{dN_{DOM}}{dt} = f_{DOM}\, grazing - remineralization_{DOM} \qquad (S4)$$

$$\frac{dN_{Detritus}}{dt} = f_{Det}\, grazing + mortality - remineralization_{Detritus} \qquad (S5)$$

The net phytoplankton growth ($growth_{Phyto}$) is the difference between the amount of nitrate fixed by photosynthesis and the
internal respiration of the phytoplankton:

$$growth_{Phyto} = (lim_{temp} lim_{NO3} lim_{Irr} PC_{max} - lim_{temp} b_{resp,Phyto}) N_{Phyto} \qquad (S6)$$

The phytoplankton parameters are tuned to represent a diatom population. $PC_{max} = 1.25$ d^{-1} is the maximum photosynthetic
rate at 0°C. Photosynthesis is limited by light and nutrient availability ($K_{NO3} = 2.5$ umolNO$_3$ kg^{-1}, see equation detailed in
(Stock et al., 2014) and increases with temperature (k$_{temp}$ = 0.063, (Eppley, 1972), equivalent to a Q10 of 1.88). $b_{resp,Phyto} =$
0.05 d^{-1} is the basal respiration rate of phytoplankton at 0°C and also increases with a Q10 of 1.88.
Zooplankton graze on phytoplankton and respire according to:

$$grazing = lim_{temp} I_{max} N_{Phyto}/(N_{Phyto} + k_I) N_{Zoo} \qquad (S7)$$

$$respiration = min(lim_{temp} b_{resp,Zoo} N_{Zoo}, \varepsilon\, grazing) \qquad (S8)$$

The zooplankton parameters are tuned to represent a medium–sized copepod population. $I_{max} = 0.57$ d^{-1} is the maximum ingestion rate and $b_{resp} = 0.008$ d^{-1} is the basal respiration rate at 0°. $k_I = 1.25$ umolN kg^{-1} is the feeding half–saturation concentration. Grazing and respiration also increase with temperature (Q10 of 1.88). $\varepsilon = 0.4$ is the maximum zooplankton growth efficiency. Respiration ($lim_{temp}b_{resp,Zoo}N_{Zoo}$) cannot be higher than the amount of food assimilated ($\varepsilon\ grazing$). If this is the case, the excess is counted as a mortality flux turning zooplankton into detritus:

$$mortality = max(0, lim_{temp}b_{resp}N_{Zoo} - \varepsilon\ grazing) \tag{S9}$$

The organic matter that is not assimilated is egested and excreted in the form of dissolved organic matter and detritus in respective fractions ($f_{DOM} = 0.45, f_{Det} = 0.15$, such that $\varepsilon + f_{DOM} + f_{Det} = 1$). Dissolved organic matter and detritus are remineralised into nitrate:

$$remineralization_{DOM} = -\boldsymbol{\gamma}_{DOM}lim_{temp}N_{DOM} \tag{S10}$$

$$remineralization_{Detritus} = -\boldsymbol{\gamma}_{Detritus}lim_{temp}N_{Detritus} \tag{S11}$$

Where $\boldsymbol{\gamma}_{DOM} = 0.011$ d^{-1} et $\boldsymbol{\gamma}_{Detritus} = 0.0028$ d^{-1} are the remineralization rates for dissolved organic matter and detritus. Because the experiment only lasts a few days, remineralization is weak and the model results are not sensitive to these parameters.

The model is forced between 08-05-2021 and 08-11-2021 by the temperatures and light intensity measured during the experiment. To compare the model outputs with the observations, a ratio of $C{:}N = 106{:}16$ molC molN^{-1} (Redfield, 1934) is used to convert the amount of nitrogen in the different pools into carbon, while a ratio of $ChlA{:}C = 0.005$ gChlA gC^{-1} (matching the ratio observed during the first chlorophyll measurements on 08-06-2021), is used to convert the amount of carbon into chlorophyll.

The model is initialized with a concentration of nitrate $N_{NO3} = 45$ umol kg^{-1}, phytoplankton $N_{Phyto} = 5$ umol kg^{-1} and zooplankton $N_{Zoo} = 0.05$ umol kg^{-1} to match the experimental measurements on 08-05-2021 and 08-06-2021. In particular, the initial phytoplankton concentration is derived from chlorophyll observations. The uncertainty associated with these initial conditions is assessed using the Monte–Carlo method by performing 1000 sensitivity experiments, randomly varying the initial concentrations within a range of ± 20 % around the values given above.

1.3 Polymerase Chain Reaction (PCR) Amplification

After DNA was extracted from each sample, PCR was used to amplify the hypervariable V4 region of the 18S rRNA gene. The full primers used were:

515F – 5' **TCGTCGGCAGCGTCAGATGTGTATAAGAGACAG**GTGYCAGCMGCCGCGGTAA 3' (Caporaso et al., 2011) and

951R – 5' **GTCTCGTGGGCTCGGAGATGTGTATAAGAGACAG**TTGGYRAATGCTTTCGC 3' (Lepère et al., 2016; Mangot et al., 2013), with bolded bases representing the overhang added for compatibility with Illumina indexing kits. PCR reagents were added to the extracted DNA according to **Table S3** for 30 μL reactions. Molecular grade water was used as the negative control. The PCR program used was a 98° C step for 30 s, followed by 30 cycles of 98° C for 10 s, 55° C for 30 s, 72° C for 30 s, and a final elongation step at 72° C for 5 min. The amplicon product was visualized on a 1 % agarose gel to check for quality and contamination before sequencing. PCR amplicons were then purified using Ampure XP beads with a 0.8:1 bead:DNA ratio and quantified using PicoGreen fluorescence (Molecular Probes, Eugene, OR).

2 Analysis

2.1 Comparison of uptake rate measurements to historical Chesapeake Bay data

Maximum C and N transport rates both occurred on day 5, concurrent with other peak bloom measurements. Peak ρ_{HCO3-} in this study were higher than average observed summer rates in the lower bay; past measurements ranged from 2–35 μM C d^{-1}, with averages closer to ~10 μM C d^{-1} (Flemer, 1970; Marshall and Nesius, 1996). Instead, maximum ρ_{HCO3-} values were more similar to those observed in the upper and central bay of up to ~100–200 μM C d^{-1} during the spring and fall diatom maxima (Flemer, 1970; Marshall and Nesius, 1996; Sellner, 1983). Peak ρ_{NO3-} was consistently higher than the up to ~6 μM N d^{-1} reported in previous studies (Bradley et al., 2010; Bronk et al., 1998; Glibert et al., 1991, 1995).

N transport in this study was determined based on NO_3^- transport rate (ρ_{NO3-}), while previous studies have used multiple N tracers to measure total dissolved N transport (ρ_{TDN}). ρ_{TDN} and relative ρ_{NO3-} are impacted by factors such as substrate availability and community composition (Bradley et al., 2010; Cochlan and Bronk, 2003; Dortch, 1990; Lomas and Glibert, 1999). Notably, the only previous studies in which ρ_{TDN} was similar to or exceeded this study's ρ_{NO3-} measured high NH_4^+ transport rates (Bradley et al., 2010; Bronk et al., 1998; Mulholland et al., 2018), which the authors attributed to summer dinoflagellate blooms. Glibert et al. (Glibert et al., 1995) also found that although the lower bay is characterized by lower ρ_{TDN} and $[NO_3^-]$, lower bay communities showed a stronger preference for NO_3^-, which the authors attributed to the diatom community. These authors observed much higher ρ_{NO3-} and stronger NO_3^- preference during blooming periods. The high observed ρ_{NO3-} rates from the current study can be explained given the low NH_4^+ concentrations ($[NH_4^+]$ = 0.7 nM in the surface waters of our study site) (Ward, 2023), high initial $[NO_3^-]$, and previously stated evidence of a diatom bloom.

In order to compare specific uptake rates to previous studies, we also normalized C transport using Chl–a concentrations (V_{C_Chla}). Unlike V_{HCO3-}, day 5 V_{C_Chla} rates were more than two times those of day 4 and had variable late–bloom patterns (**Fig. S8**). The average maximum value in each carboy (regardless of timing) was $195 \pm 50\ \mu g$ C μg Chl–a^{-1} d^{-1}, comparable to previously observed values up to ~150–200 μg C μg Chl–a^{-1} d^{-1} (Adolf et al., 2006; Flemer, 1970; Harding et al., 2002). High maximum V_{C_Chla} in this study match seasonal trends of a summer V_{C_Chla} peak previously observed in Chesapeake Bay, attributed to nutrient limitation and high grazing control over the summer phytoplankton community (Adolf et al., 2006; Malone et al., 1996). i.e., when there is an input of nutrients, the phytoplankton are able to rapidly assimilate C despite the low Chl–a due to grazing, leading to high V_{C_Chla}.

It should be noted that both absolute transport and specific N uptake rates may be overestimated after day 5, as ambient [NO$_3^-$] became depleted. Therefore, these later rates should be considered potential uptake rates, as the added ^{15}N tracer contributed significantly to the nutrient pool (**Table S6**). Similarly for carbon, a constant DIC concentration was assumed and the At%DIC$_{natural}$ is based on the ^{15}N incubations, both of which can impact the calculated ρ_{HCO3-}. However, it is unlikely that any temporal patterns observed in the transport or specific uptake rates were altered by these factors. ρ_{NO3-} values were very low following the bloom peak when substrate was the most depleted and the most susceptible to stimulation by the ^{15}N tracer additions. ρ_{HCO3-} were also low following the bloom peak and carboys were uncapped and gently mixed during each sampling event, allowing for DIC to equilibrate with atmospheric concentrations.

2.2 NPZ Model Simplifications

Simplifications in the model led to slight deviations between model outputs and observations. Differences in modeled Chl–a and POM concentrations may be due to the model not accounting for the full range of phytoplankton POC:Chl–a and changes as the phytoplankton community shifted during the bloom. Though the phytoplankton community was parameterized to match diatoms, the actual observed phytoplankton POC:Chl–a in Chesapeake Bay ranges 40–90, which is much lower than the 200 $\pm$ 20% used in the model and resulted in an overestimation of POM based on Chl–a. The daily temporal resolution of the model may have also resulted in a less steep decrease in [NO$_3^-$] than observed between 06:00 and noon day 5, leading to an overestimation of phytoplankton biomass and Chl–a following the peak bloom. Despite these minor deviations, the consensus between observations and a simplified NPZ model demonstrates that even a diverse diatom assemblage acts in accordance with globally averaged diatom behavior under blooming conditions.

Notably, the model was initialized using only the observed day 2 Chl–a and NO$_3^-$ concentrations and a range of POC:Chl–a ratios. The physiological parameters of the phytoplankton and zooplankton in the NPZ model were tuned according to the global COBALTv2 model (Stock et al., 2020). This avoided over–parameterization of the model and indicates that the response of the microbial eukaryotic community to a sudden influx of nutrients is consistent across ecosystems. Furthermore, this

contrasts with previous studies which have found a decoupling of diatoms and copepods in the open ocean (Lima-Mendez et al., 2015) and suggests that the diatom community in a shallow, coastal environment can be controlled both by bottom–up and top–down factors.

2.3 *Karenia mikimotoi*

150   In addition to fucoxanthin, *Karenia mikimotoi* also contains the fucoxanthin derivatives 19'–butanoyloxyfucoxanthin and 19'–hexanoyloxyfucoxanthin (Huang et al., 2021; Wright and Jeffrey, 1987), as well as the *Karenia*–specific accessory pigment gyroxanthin–diester (Li et al., 2010; Richardson and Pinckney, 2004) that diatoms do not (Stauber and Jeffrey, 1988). Huang et al. (Huang et al., 2021) observed that 19'–butanoyloxyfucoxanthin and 19'–hexanoyloxyfucoxanthin can constitute 1.5–4.6 % and 0.9–2.7 %, respectively, of total pigments in *K. mikimotoi*. 19'– butanoyloxyfucoxanthin concentrations were 0 μg L^{-1}

155   throughout duration of the mesocosm experiments and both 19'–hexanoyloxyfucoxanthin and gyroxanthin–diester had minor peaks during the early bloom, which dropped to 0 μg L^{-1} before the day 5 bloom peak (**Fig. S11**). *K. mikimotoi* also grows slower than diatoms and tends to be more competitive in lower nutrient environments, with much lower expected ρ_{NO3^-} than those observed in this study (Huang et al., 2020; Li et al., 2010).

160   Given its nutrient uptake and growth strategies, the mesocosms had the best growth conditions for *K. mikimotoi* during the decline of the diatom bloom, as they can utilize a variety of N substrates including the organic nutrients released from decaying diatoms (Brand et al., 2012; Huang et al., 2020; Li et al., 2010). Pairwise comparison showed that the mid– and late–bloom diatom and dinoflagellate relative abundances were negatively correlated (Pearson correlation, $r^2 = 0.88$, $p = 3.3 \times 10^{-6}$). However, dinoflagellate relative abundances were high in both mid– and late–bloom samples, while diatom relative

165   abundances are highest during the mid–bloom. Due to the interdependence of relative abundances, the correlation between diatoms and dinoflagellates could result from diatom abundance decreasing with minimal change in absolute dinoflagellate abundance. Additionally, the accessory pigment data do not support a late–bloom increase in dinoflagellate biomass. Instead, we suggest that the apparent high relative abundance of dinoflagellates is an issue of 18S gene copy number.

170 **3 Supplementary Tables**

Measurement	Detection limit (DL)	Precision
[NO_2^-]	0.25 μM	±0.034 μM
[Silicate]	0.5 μM	±0.26 μM
[PO_4^{3-}]	0.1 μM	±0.05 μM
NOxBox ([NO_2^- + NO_3^-])	0.2–0.3 μM or 0.1–0.15 nmol N	±0.11 μM or ±0.056 nmol N
POC	4.00 μg	±1.01 μg
PON	4.67 μg	±1.23 μg
$\delta^{13}C$	n/a	0.52 ‰
$\delta^{15}N$	n/a	0.41 ‰

Table S1: Detection limit (DL) and precision measurements for nutrients and mass spec analyses. DL was based on the lowest measurable standard and is represented by a range if DL varied between runs. Precision calculations based on the average deviation of observed standard measurements from expected values.

Pigment	Average effective limit of detection (μg pigment L^{-1})	Average effective limit of quantification (μg pigment L^{-1})
Chlorophyll a	0.009	0.030
Fucoxanthin	0.004	0.013
Peridinin	0.004	0.012
Zeaxanthin	0.003	0.011
19'Butanoyloxy–fucoxanthin	0.004	0.012
19'Hexanoyloxy–fucoxanthin	0.003	0.009
Gyroxanthin–diester	0.003	0.008

175 **Table S2:** Average effective detection limit and effective limit of quantification for HPLC pigment analyses.

Reagent	Concentration	Volume Per Sample (μL)
Buffer	10x	6.0
dNTP	10 mM	0.6
515F Primer	20 μM	0.75
951R Primer	20 μM	0.75
Phusion Taq	2 U/μL	0.2
Molecular Grade Water		20.7
DNA or Negative Control		1.0

Table S3: Polymerase chain reaction (PCR) mixed reagent details.

Carboy	ρ_{HCO3} (μM C d^{-1})	V_{HCO3} day 4 (d^{-1})	V_{HCO3} day 5 (d^{-1})	ρ_{NO3} (μM N d^{-1})	V_{NO3} day 4 (d^{-1})	V_{NO3} day 5 (d^{-1})
A	141.6 ± 31.8	1.0 ± 0.057	0.71 ± 0.054	26.3 ± 13.2	0.77 ± 0.18	1.1 ± 0.21
B	187.2 ± 58.8	1.0 ± 0.076	0.94 ± 0.18	28.5 ± 4.28	1.1 ± 0.050	1.2 ± 0.039
C	229.3 ± 80.6	1.1 ± 0.040	0.94 ± 0.15	26.6 ± 11.1	0.90 ± 0.044	1.1 ± 0.089
avg.	**186.0 ± 64.7**	**1.0 ± 0.060**	**0.86 ± 0.16**	**27.1 ± 8.95**	**0.91 ± 0.16**	**1.1 ± 0.12**

180   **Table S4:** Mid-bloom transport (ρ) and specific uptake rates (V) for each carboy. Full mesocosm Kruskal–Wallis analysis for V in figure S4.

Sample Name	Carboy	Rep	Date Collected	Day	Bloom Timing
CB2021_1	inoculum	1	4-Aug-21	0	- -
CB2021_2	inoculum	2	4-Aug-21	0	- -
CB2021_5	A	1	6-Aug-21	2	early
CB2021_7	B	1	6-Aug-21	2	early
CB2021_9	C	1	6-Aug-21	2	early
CB2021_11	A	1	7-Aug-21	3	early
CB2021_13	B	1	7-Aug-21	3	early
CB2021_15	C	1	7-Aug-21	3	early
CB2021_16	C	2	7-Aug-21	3	early
CB2021_17	filtered SW	1	4-Aug-21	0	- -
CB2021_19	A	1	8-Aug-21	4	mid
CB2021_21	B	1	8-Aug-21	4	mid
CB2021_23	C	1	8-Aug-21	4	mid
CB2021_25	A	1	9-Aug-21	5	mid/peak
CB2021_27	B	1	9-Aug-21	5	mid/peak
CB2021_29	C	1	9-Aug-21	5	mid/peak
CB2021_30	C	2	9-Aug-21	5	mid/peak
CB2021_31	A	1	10-Aug-21	6	late
CB2021_34	B	1	10-Aug-21	6	late
CB2021_37	C	1	10-Aug-21	6	late
CB2021_38	C	2	10-Aug-21	6	late
CB2021_40	A	1	11-Aug-21	7	late
CB2021_43	B	1	11-Aug-21	7	late
CB2021_46	C	1	11-Aug-21	7	late

Table S5: 18S rRNA gene sample names and metadata.

185

Day No.	^{13}Carbon	^{15}Nitrogen			
	All Carboys	Carboy A	Carboy B	Carboy C	Avg.
2	9.98%	8.67%	8.54%	9.08%	**8.76%**
3	9.98%	9.00%	9.12%	10.23%	**9.45%**
4	9.98%	10.22%	9.01%	9.74%	**9.65%**
5	9.98%	13.06%	11.59%	13.52%	**12.73%**
6	10%	72.96%	77.04%	78.24%	**76.08%**
7	10%	84.63%	93.93%	91.87%	**90.14%**

Table S6: The mole percent enrichment of the transport rate incubations. Carbon enrichments assume a constant 1.8 mM dissolved inorganic carbon (DIC) concentration and nitrogen enrichments are calculated using the corresponding [NO_3^-].

190

	Kinetic Threshold	Stoichiometric Thresholds	
Nitrogen	[NO_3^-] $\leq 1.0\ \mu$M	N:P < 10	N:Si < 1
Phosphorus	[PO_4^{3-}] $\leq 0.2\ \mu$M	N:P > 22	Si:P > 22
Silicate	[SiO_4^{4-}] $\leq 2.0\ \mu$M	N:Si > 1	Si:P < 10

Table S7: The kinetics– and stoichiometry–based thresholds for diatom nutrient limitation as outlined in Liang et al. (2019). Nutrients were only considered limiting if they met all three thresholds for limitation at a given timepoint.

4 Supplementary Figures

195
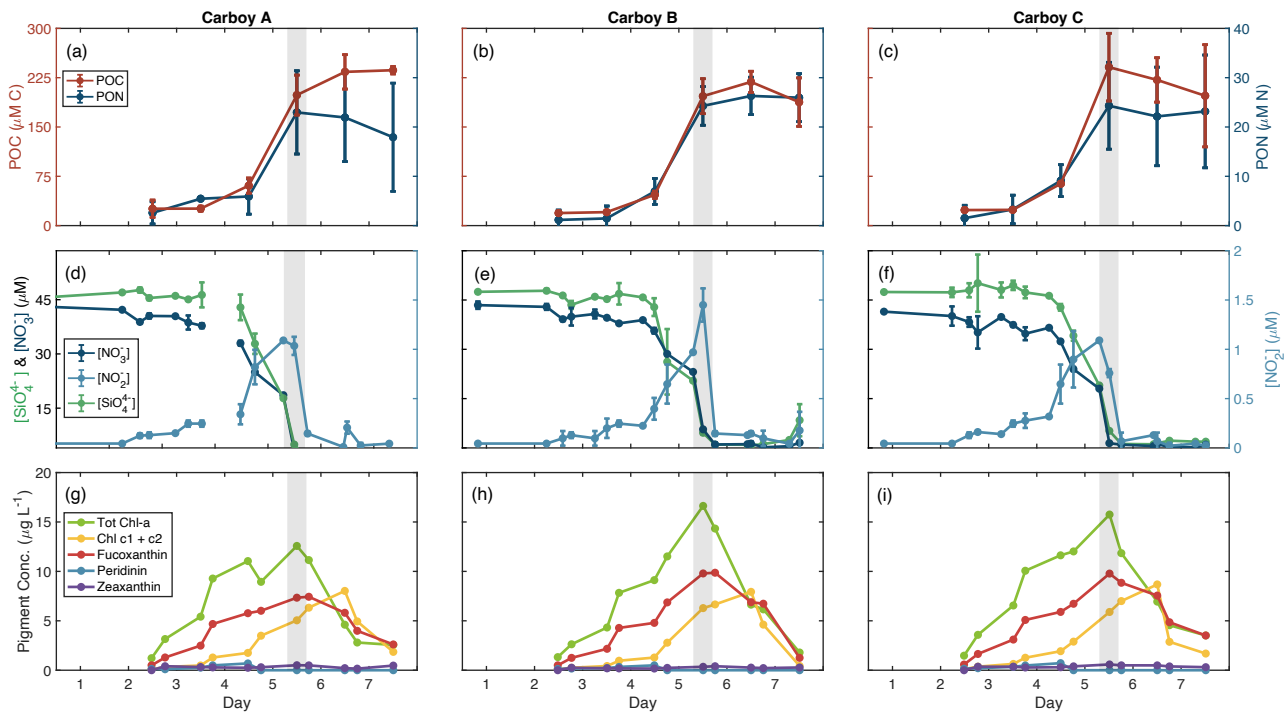
Figure S1: Biogeochemical data for all carboys (a–c) Particulate organic carbon (POC) and nitrogen (PON) are shown in red and blue, respectively, for each carboy. (d–f) Nutrient concentrations are presented as dark blue lines for nitrate ([NO$_3^-$]), light blue lines for nitrite ([NO$_2^-$]), and green lines for silicate ([SiO$_4^{4-}$]). (g–i) Pigment concentrations for chlorophyll a (Chl–a), chlorophyll c (Chl c1 + c2), and diagnostic pigments for diatoms (fucoxanthin), dinoflagellates (peridinin), and cyanobacteria (zeaxanthin). Error bars on plots (a–f) represent
200 standard deviation of sample replicates. No error bars are plotted for pigments because only duplicate samples were taken. Time is shown as days since mesocosm inoculation. The grey shaded region indicates the peak bloom.
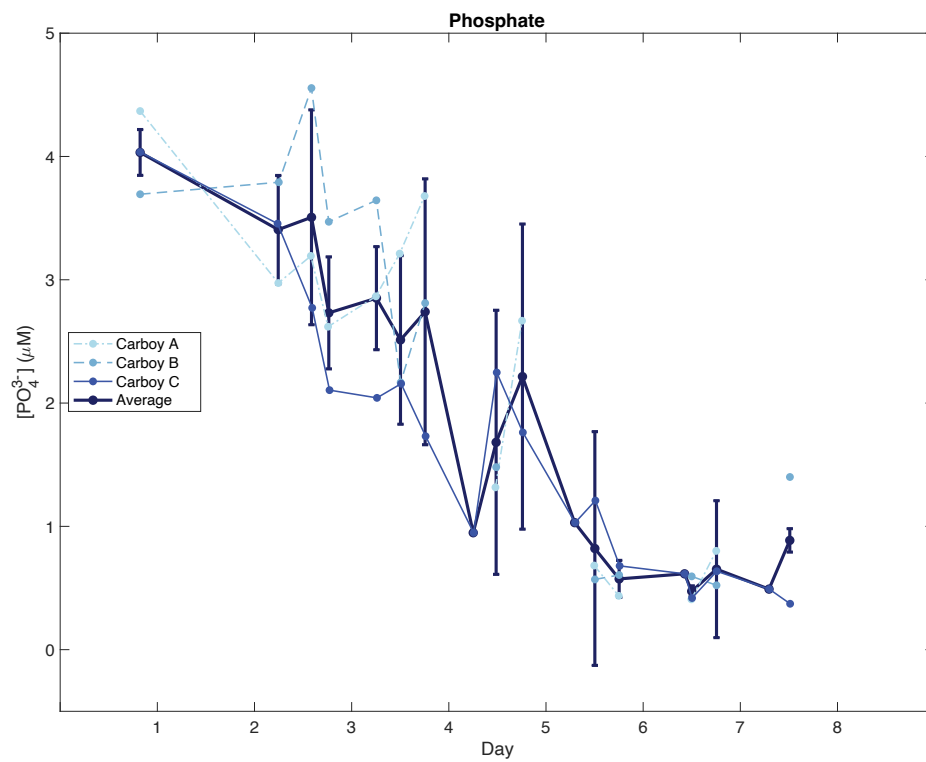
Figure S2: Phosphate concentrations ([PO$_4^{3-}$]) for each carboy are plotted in thin lines and the average concentration for all carboys is plotted in a thick solid line. Line type denotes carboy. Error bars for average [PO$_4^{3-}$] represent the propagation of the standard deviation for each carboy. Time is shown as days since mesocosm inoculation.

205
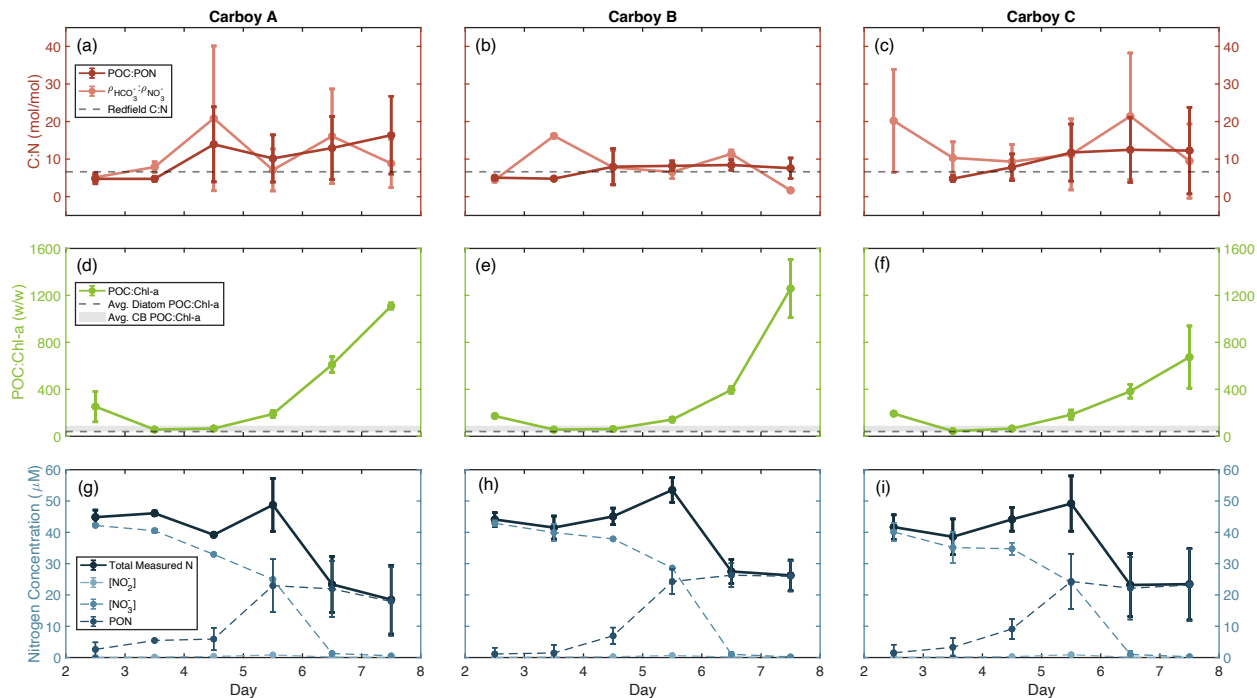
Figure S3: Nutrient and pigment ratios, and nitrogen mass balance for all carboys. (a–c) Carbon–to–Nitrogen (C:N) ratios are plotted in terms of both particulate organic matter (POC:PON, red solid lines) and transport rates (ρ_{HCO3-}:ρ_{NO3-}, pink solid lines) for each carboy. Grey dashed lines show Redfield (Redfield, 1934) C:N (i.e.; 106:16). Error bars are missing for early C:N samples if only one particulate organic nitrogen (PON) triplicate was above detection limit. (d–f) Particulate organic carbon–to–chlorophyll a (POC:Chl–a) ratios are plotted in green and compared against the expected Chesapeake Bay (Avg. CB) POC:Chl–a, the grey shaded region, and average diatom POC:Chl–a, the grey dashed line. (g–i) Concentrations of individual nitrogen pools: nitrite ($[NO_2^-]$), nitrate ($[NO_3^-]$), and PON as dashed lines. Total measured N ($[NO_2^-]$ + $[NO_3^-]$ + PON) is plotted as a solid line. All error bars represent the standard deviation of sample replicates. Time is shown as days since mesocosm inoculation.
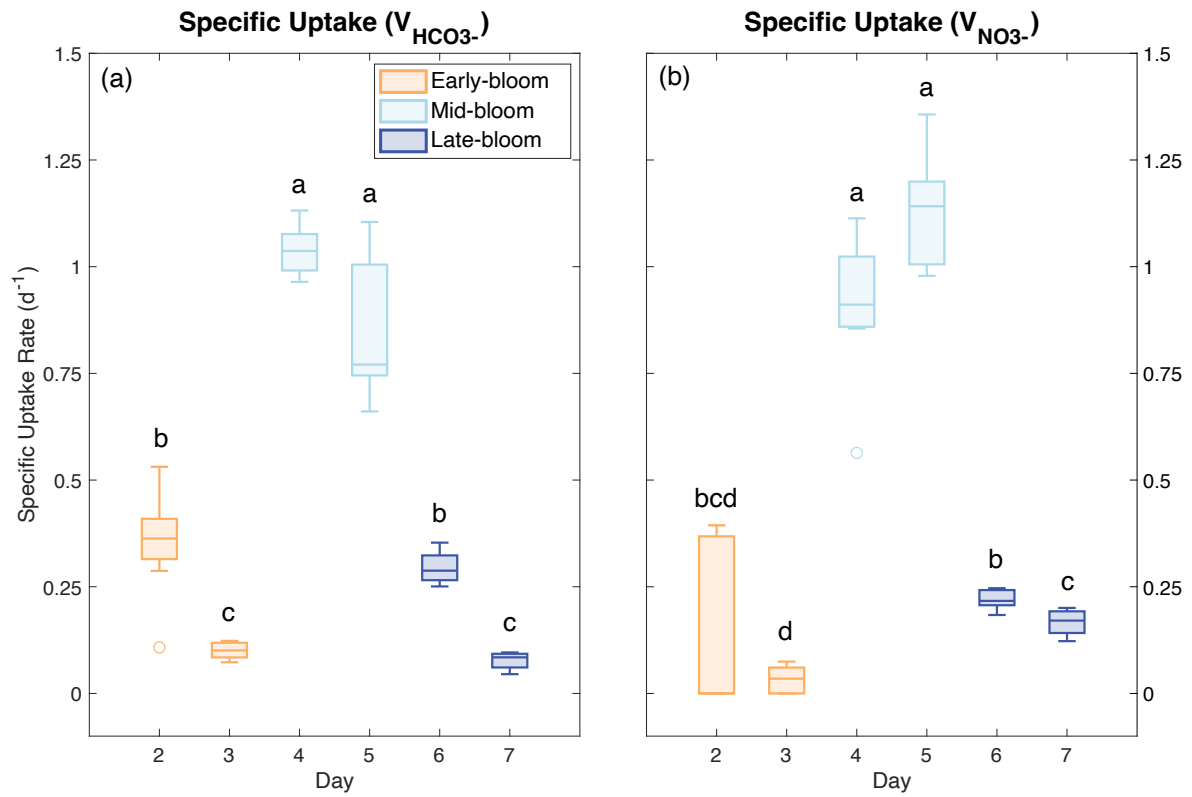
Figure S4: Temporal analysis of specific uptake rates. The specific uptake rates for (a) carbon (V_{HCO3-}) and (b) nitrogen (V_{NO3-}) from all carboys were grouped by day for the above boxplots. A Kruskal–Wallis test found both V_{HCO3-} and V_{NO3-} to vary significantly with day ($p = 1.4 \times 10^{-8}$ and $p = 5.6 \times 10^{-8}$, respectively). Boxes are colored by early–, mid–, and late–bloom, and letter labels above each box represent significantly different groupings (Bonferroni–adjusted pairwise comparisons, $p < 0.01$). For each box, the inner line is the median value, the top and bottom edges are the upper and lower quartiles, and the whiskers show the minimum and maximum non–outlier values.
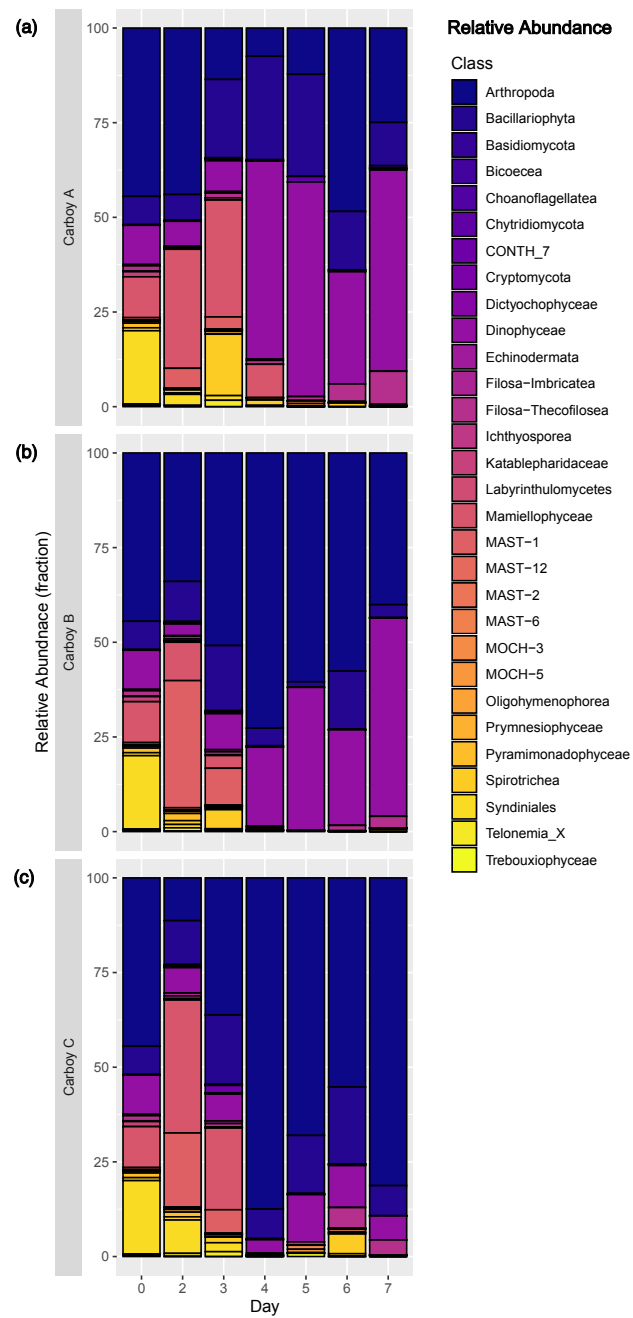
Figure S5: Community succession of full eukaryotic community. Relative abundance of all non–bacterial 18S–derived OTUs colored by taxonomic class for (a) carboy A, (b) carboy B, and (c) carboy C. Day corresponds to the number of days since mesocosm inoculation.
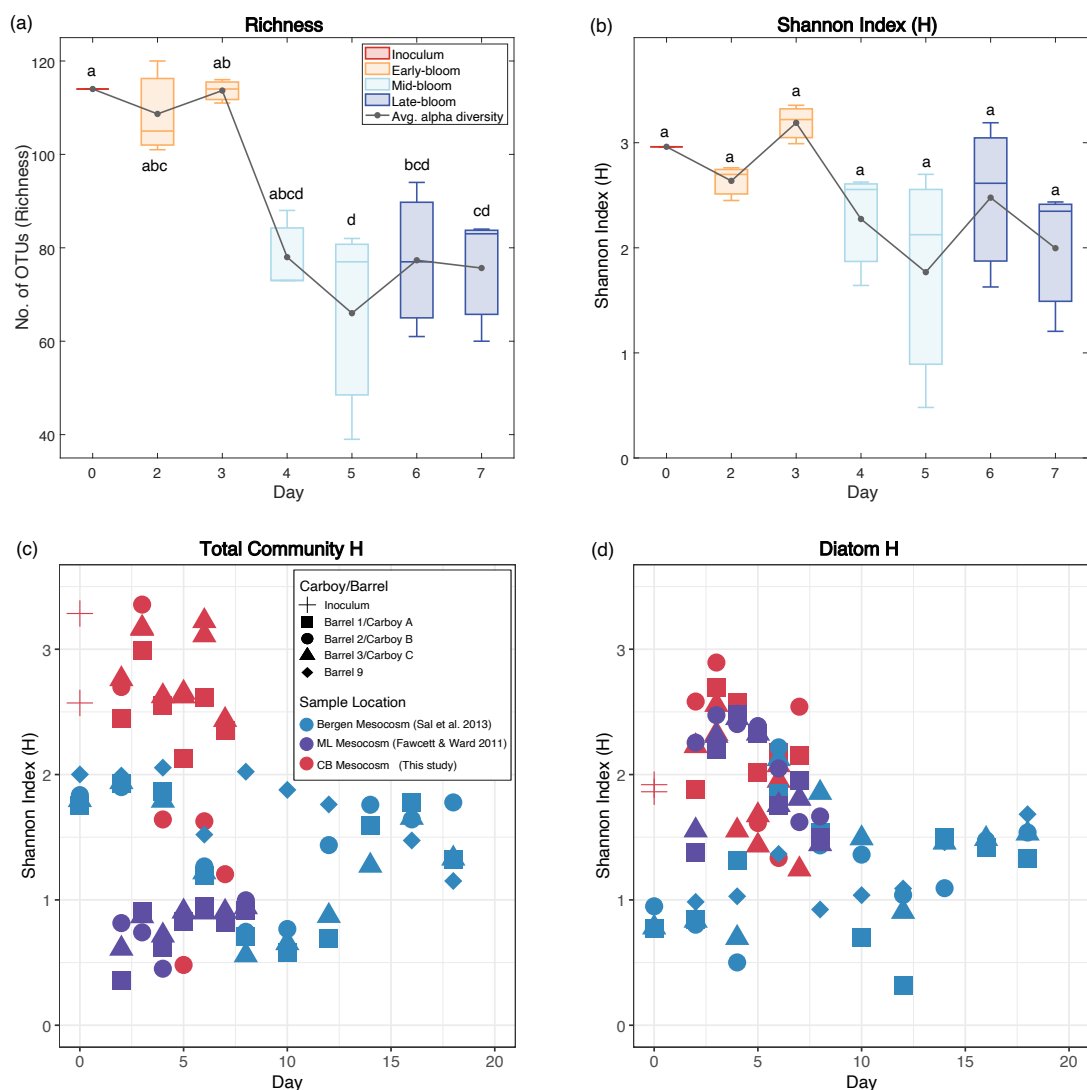
Figure S6: Temporal trends in alpha diversity. Boxplots of the (a) number of OTUs (richness) and (b) Shannon Index (H) for all carboys over time. A one–way ANOVA found richness to vary significantly with day ($p = 9.29 \times 10^{-4}$) while H did not ($p = 0.144$). Boxes are colored by early–, mid–, and late–bloom, and letter labels above each box represent significantly different groupings (Tukey's HSD family–wise comparisons with 95% confidence). For each box, the inner line is the median value, the top and bottom edges are the upper and lower quartiles, and the whiskers show the minimum and maximum non–outlier values. Grey lines represent the average value. Day corresponds to the number of days since mesocosm inoculation, with day 0 represented by the single merged inoculum sample. This study (CB) was compared to other mesocosms performed in the Moss Landing (ML), California upwelling system (Fawcett and Ward, 2011) and Bergen, Norway (Sal et al., 2013). Individual (unmerged) sample H is plotted for (c) the whole non–metazoan eukaryotic community and (d) the diatom community. The Bergen mesocosms are plotted in blue, ML in purple, and CB in red. Shape indicates individual mesocosm.

235
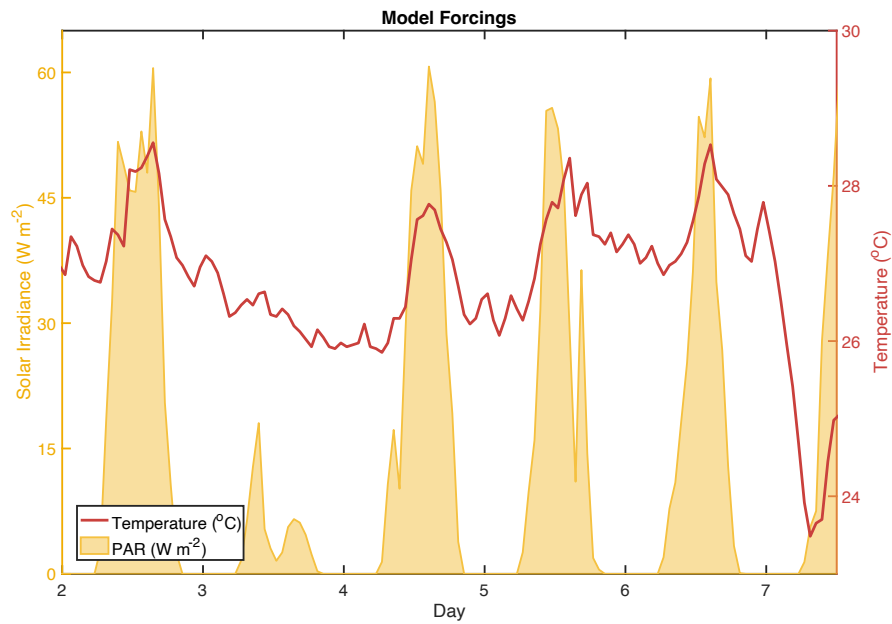
Figure S7: Light and temperature. Continuous light (yellow shaded region) and temperature (red line) measurements are plotted for the duration of the mesocosm experiment. Duplicate loggers were combined and measurements were averaged along hourly intervals.
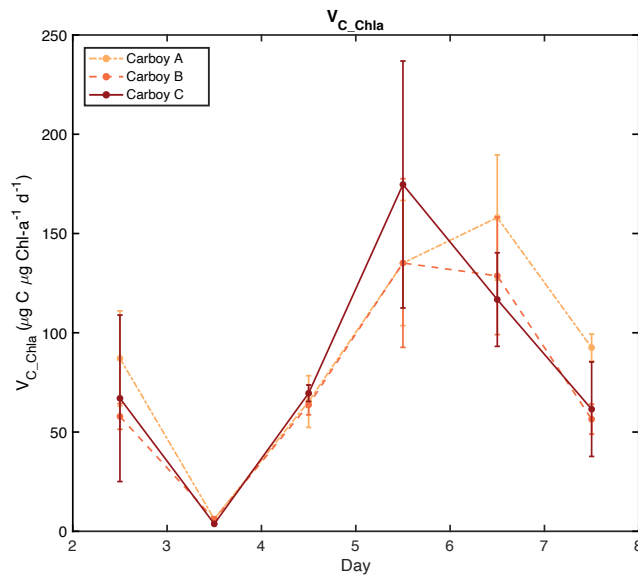
Figure S8: Chlorophyll–a–normalized carbon uptake rates (V_{C_Chla}). Carbon transport rates were normalized by Chl–a concentration (V_{C_Chla}, μg C μg Chl–a^{-1} d^{-1}). Line type and color indicate carboy. Error bars depict standard devation of replicate measurements.

240
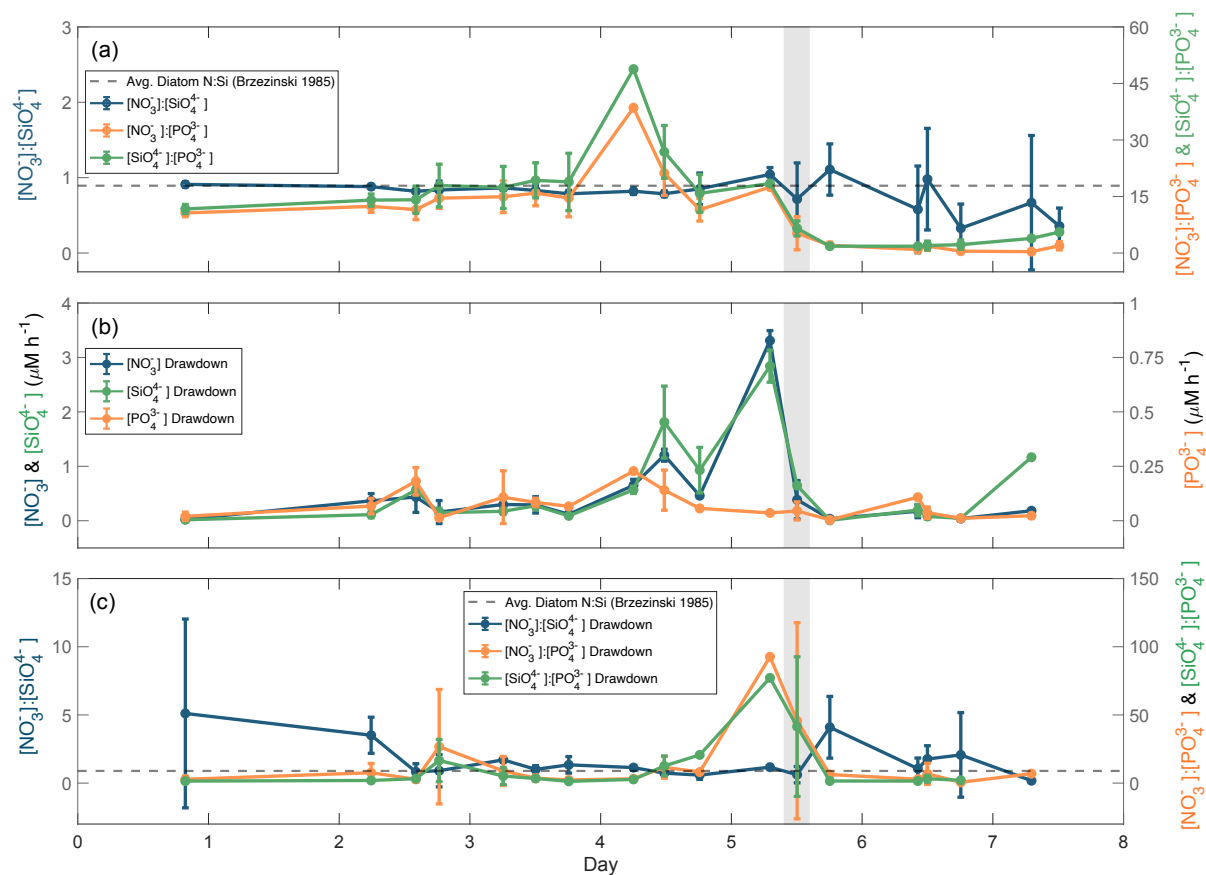
Figure S9: Average observed nutrient ratios and diatom nutrient quotas. (a) Ambient nitrate ($[NO_3^-]$), silicate ($[SiO_4^{4-}]$), and phosphate ($[PO_4^{3-}]$) ratios. $[NO_3^-]:[SiO_4^{4-}]$ in blue, $[NO_3^-]:[PO_4^{3-}]$ in orange, and $[SiO_4^{4-}]:[PO_4^{3-}]$ in green are plotted alongside the average nitrogen-to-silica ratio (N:Si) of diatom particulate matter, 0.8929 (Brzezinski, 1985). (b) Drawdown rates for $[NO_3^-]$ in blue, $[SiO_4^{4-}]$ in green, and $[PO_4^{3-}]$ in orange and (c) ratios of drawdown rates $[NO_3^-]:[SiO_4^{4-}]$ drawdown in blue, $[NO_3^-]:[PO_4^{3-}]$ drawdown in orange, and $[SiO_4^{4-}]:[PO_4^{3-}]$ drawdown in green, alongside average diatom N:Si. Drawdown rates are calculated for each timepoint (t) as $[nutrient]_{t+1} - [nutrient]_t$. All error bars represent the standard deviation between carboys. Time is shown as days since mesocosm inoculation.

245
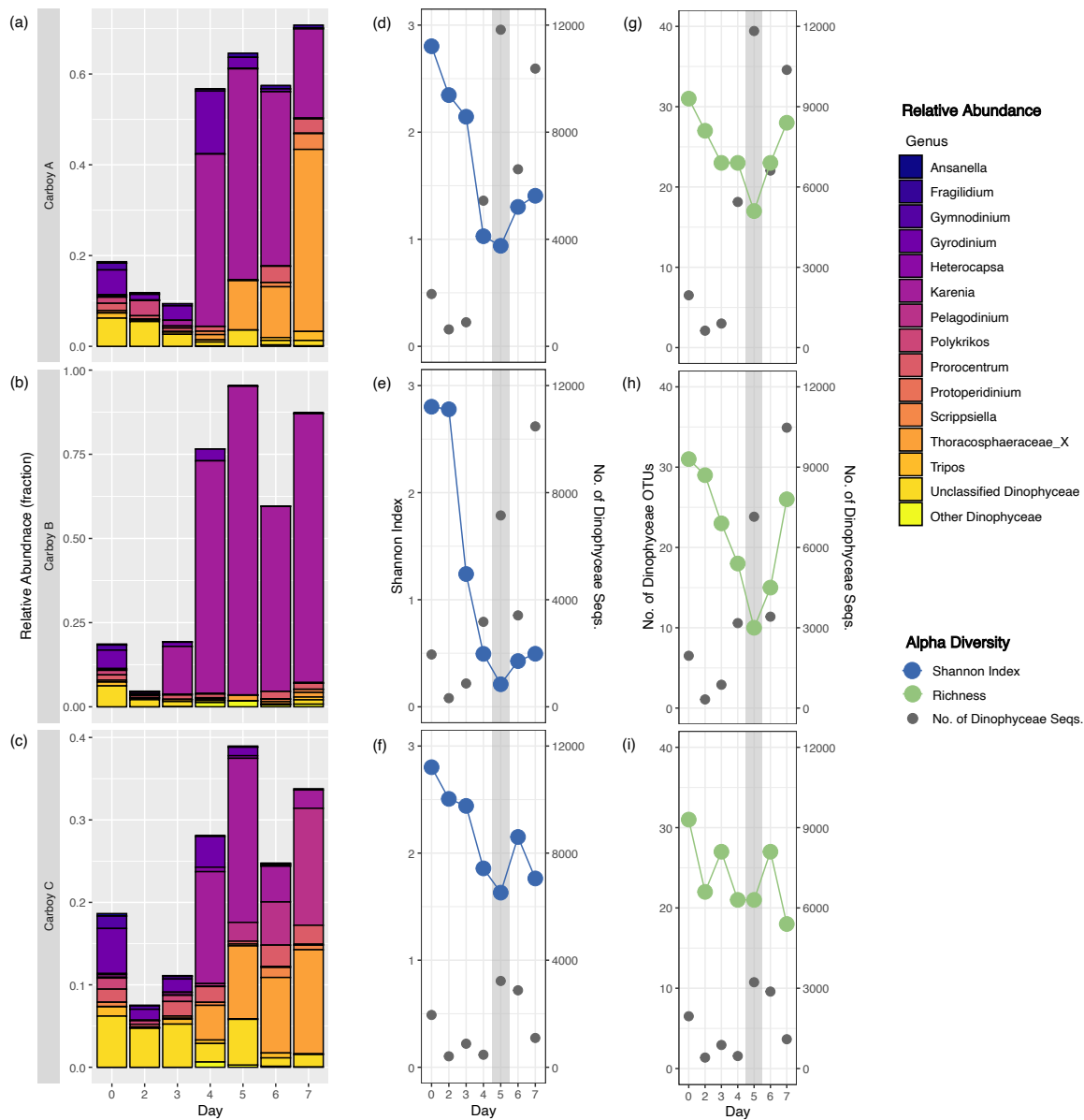
250 **Figure S10: Dinoflagellate (Dinophyceae) community succession and alpha diversity.** (a–c) Relative abundance of dinoflagellate OTUs (fraction of the total non–metazoan community) for each carboy, colored by and outlined around genus. Day corresponds to the number of days since mesocosm inoculation, with day 0 for each carboy represented by the same merged inoculum sample. "Unclassified Dinophyceae" are OTUs which were ≥ 97% similar to a PR^2 reference sequence, but were not taxonomically classified at the genus level. "Other Dinophyceae" are OTUs which were < 97% similar to a PR^2 reference sequence. Y–axis range is variable. (d–i) Shannon alpha diversity 255 (blue), number of dinoflagellate OTUs (i.e. richness) (green), and the number of dinoflagellate sequences (grey) on the same "Day" scale. The grey shaded region indicates the peak bloom.
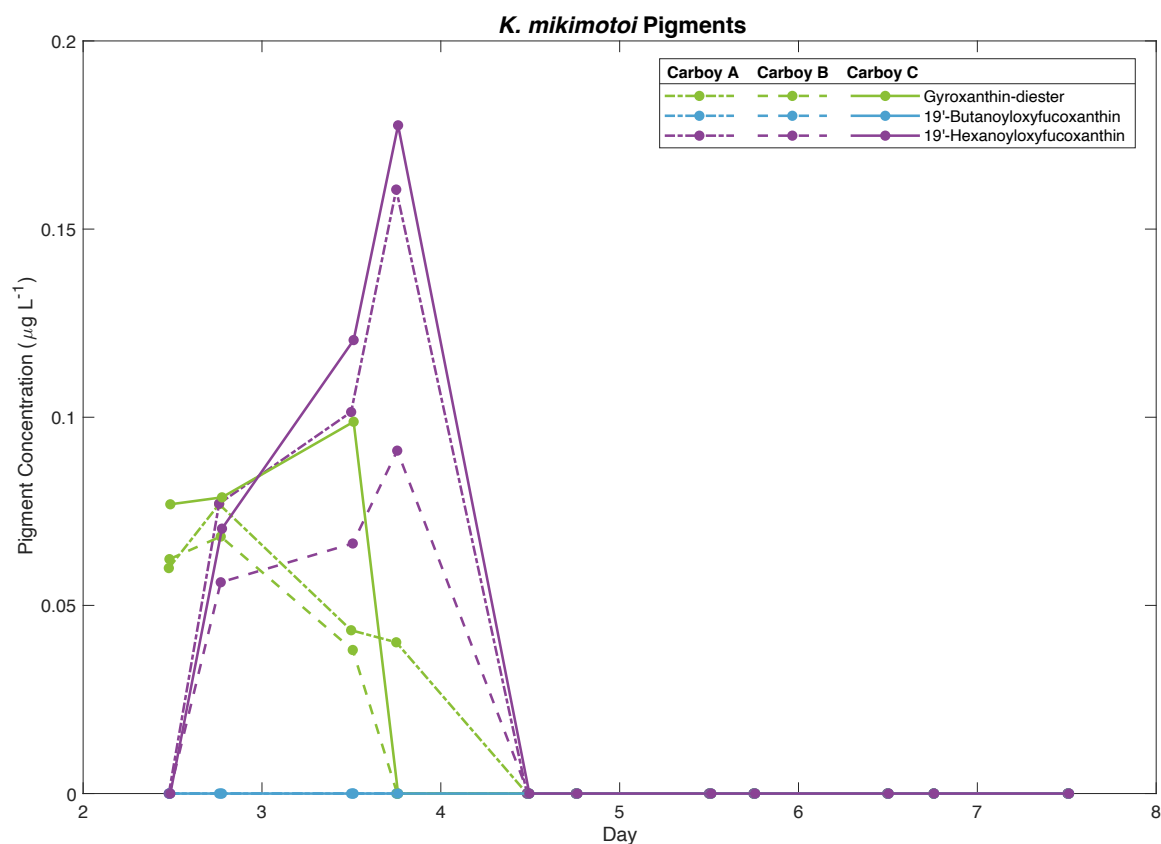
Figure S11: *Karenia mikimotoi* **accessory pigments.** Gyroxanthin–diester is plotted in green, 19'Butanoyloxyfucoxanthin in light blue, and 19'Hexanoyloxyfucoxanthin in dark purple lines. Line type denotes carboy. Day corresponds to the number of days since mesocosm inoculation.

References

Adolf, J. E., Yeager, C. L., Miller, W. D., Mallonee, M. E., and Harding, L. W.: Environmental forcing of phytoplankton floral composition, biomass, and primary productivity in Chesapeake Bay, USA, Estuar. Coast. Shelf Sci., 67, 108–122, https://doi.org/10.1016/j.ecss.2005.11.030, 2006.

Bradley, P. B., Lomas, M. W., and Bronk, D. A.: Inorganic and Organic Nitrogen Use by Phytoplankton Along Chesapeake Bay, Measured Using a Flow Cytometric Sorting Approach, Estuaries Coasts, 33, 971–984, https://doi.org/10.1007/s12237-009-9252-y, 2010.

Brand, L. E., Campbell, L., and Bresnan, E.: Karenia: The biology and ecology of a toxic genus, Harmful Algae, 14, 156–178, https://doi.org/10.1016/j.hal.2011.10.020, 2012.

Bronk, D. A., Glibert, P., Malone, T., Banahan, S., and Sahlsten, E.: Inorganic and organic nitrogen cycling in Chesapeake Bay: autotrophic versus heterotrophic processes and relationships to carbon flux, Aquat. Microb. Ecol., 15, 177–189, https://doi.org/10.3354/ame015177, 1998.

Brzezinski, M. A.: The Si:C ratio of marine diatoms: Interspecific variability and the effect of some environmental variables, J. Phycol., 21, 347–357, 1985.

Caporaso, J. G., Lauber, C. L., Walters, W. A., Berg-Lyons, D., Lozupone, C. A., Turnbaugh, P. J., Fierer, N., and Knight, R.: Global patterns of 16S rRNA diversity at a depth of millions of sequences per sample, Proc. Natl. Acad. Sci., 108, 4516–4522, https://doi.org/10.1073/pnas.1000080107, 2011.

Cochlan, W. P. and Bronk, D. A.: Effects of ammonium on nitrate utilization in the Ross Sea, Antarctica: Implications for f-ratio estimates, in: Antarctic Research Series, vol. 78, edited by: DiTullio, G. R. and Dunbar, R. B., American Geophysical Union, Washington, D. C., 159–178, https://doi.org/10.1029/078ARS10, 2003.

Dortch, Q.: The interaction between ammonium and nitrate uptake in phytoplankton, Mar. Ecol. Prog. Ser., 61, 183–201, https://doi.org/10.3354/meps061183, 1990.

Eppley, R. W.: Temperature and phytoplankton growth in the sea, Fish. Bull., 70, 1063, 1972.

Fawcett, S. and Ward, B.: Phytoplankton succession and nitrogen utilization during the development of an upwelling bloom, Mar. Ecol. Prog. Ser., 428, 13–31, https://doi.org/10.3354/meps09070, 2011.

Flemer, D. A.: Primary Production in the Chesapeake Bay, Chesap. Sci., 11, 117, https://doi.org/10.2307/1350486, 1970.

Glibert, P. M., Garside, C., Fuhrman, J. A., and Roman, M. R.: Dependent coupling of inorganic and organic nitrogen uptake and regeneration in the plume of the Chesapeake Bay estuary and its regulation by large heterotrophs, Limnol. Oceanogr., 36, 895–909, 1991.

Glibert, P. M., Conley, D. J., Fisher, T. R., Jr, L. W. H., and Malone, T. C.: Dynamics of the 1990 winter/spring bloom in Chesapeake Bay, Mar. Ecol. Prog. Ser., 122, 27–43, 1995.

Harding, L. W., Mallonee, M. E., and Perry, E. S.: Toward a Predictive Understanding of Primary Productivity in a Temperate, Partially Stratified Estuary, Estuar. Coast. Shelf Sci., 55, 437–463, https://doi.org/10.1006/ecss.2001.0917, 2002.

Huang, K., Feng, Q., Zhang, Y., Ou, L., Cen, J., Lu, S., and Qi, Y.: Comparative uptake and assimilation of nitrate, ammonium, and urea by dinoflagellate Karenia mikimotoi and diatom Skeletonema costatum s.l. in the coastal waters of the East China Sea, Mar. Pollut. Bull., 155, 111200, https://doi.org/10.1016/j.marpolbul.2020.111200, 2020.

Huang, K., Zhuang, Y., Wang, Z., Ou, L., Cen, J., Lu, S., and Qi, Y.: Bioavailability of Organic Phosphorus Compounds to the Harmful Dinoflagellate Karenia mikimotoi, Microorganisms, 9, 1961, https://doi.org/10.3390/microorganisms9091961, 2021.

Lepère, C., Domaizon, I., Hugoni, M., Vellet, A., and Debroas, D.: Diversity and Dynamics of Active Small Microbial Eukaryotes in the Anoxic Zone of a Freshwater Meromictic Lake (Pavin, France), Front. Microbiol., 7, https://doi.org/10.3389/fmicb.2016.00130, 2016.

305 Li, J., Glibert, P. M., and Zhou, M.: Temporal and spatial variability in nitrogen uptake kinetics during harmful dinoflagellate blooms in the East China Sea, Harmful Algae, 9, 531–539, https://doi.org/10.1016/j.hal.2010.03.007, 2010.

Liang, Y., Zhang, G., Wan, A., Zhao, Z., Wang, S., and Liu, Q.: Nutrient-limitation induced diatom-dinoflagellate shift of spring phytoplankton community in an offshore shellfish farming area, Mar. Pollut. Bull., 141, 1–8, https://doi.org/10.1016/j.marpolbul.2019.02.009, 2019.

Lima-Mendez, G., Faust, K., Henry, N., Decelle, J., Colin, S., Carcillo, F., Chaffron, S., Ignacio-Espinosa, J. C., Roux, S.,
310 Vincent, F., Bittner, L., Darzi, Y., Wang, J., Audic, S., Berline, L., Bontempi, G., Cabello, A. M., Coppola, L., Cornejo-Castillo, F. M., d'Ovidio, F., De Meester, L., Ferrera, I., Garet-Delmas, M.-J., Guidi, L., Lara, E., Pesant, S., Royo-Llonch, M., Salazar, G., Sánchez, P., Sebastian, M., Souffreau, C., Dimier, C., Picheral, M., Searson, S., Kandels-Lewis, S., Tara Oceans coordinators, Gorsky, G., Not, F., Ogata, H., Speich, S., Stemmann, L., Weissenbach, J., Wincker, P., Acinas, S. G., Sunagawa, S., Bork, P., Sullivan, M. B., Karsenti, E., Bowler, C., De Vargas, C., and Raes, J.: Determinants of community
315 structure in the global plankton interactome, Science, 348, 1262073, https://doi.org/10.1126/science.1262073, 2015.

Lomas, M. W. and Glibert, P. M.: Interactions between NH4+ and NO3- uptake and assimilation: comparison of diatoms and dinoflagellates at several growth temperatures, Mar. Biol., 133, 541–551, 1999.

Malone, T. C., Conley, D. J., Fisher, T. R., Glibert, P. M., Harding, L. W., and Sellner, K. G.: Scales of Nutrient-Limited Phytoplankton Productivity in Chesapeake Bay, Estuaries, 19, 371, https://doi.org/10.2307/1352457, 1996.

320 Mangot, J., Domaizon, I., Taib, N., Marouni, N., Duffaud, E., Bronner, G., and Debroas, D.: Short-term dynamics of diversity patterns: evidence of continual reassembly within lacustrine small eukaryotes, Environ. Microbiol., 15, 1745–1758, https://doi.org/10.1111/1462-2920.12065, 2013.

Marshall, H. G. and Nesius, K. K.: Phytoplankton composition in relation to primary production in Chesapeake Bay, Mar. Biol., 125, 611–617, https://doi.org/10.1007/BF00353272, 1996.

325 Mulholland, M. R., Morse, R., Egerton, T., Bernhardt, P. W., and Filippino, K. C.: Blooms of Dinoflagellate Mixotrophs in a Lower Chesapeake Bay Tributary: Carbon and Nitrogen Uptake over Diurnal, Seasonal, and Interannual Timescales, Estuaries Coasts, 41, 1744–1765, https://doi.org/10.1007/s12237-018-0388-5, 2018.

Redfield, A. C.: On the proportions of organic derivatives in sea water and their relation to the composition of plankton, James Johnstone Meml. Vol. Univ. Press Liverp., 176–192, 1934.

330 Richardson, T. L. and Pinckney, J. L.: Monitoring of the toxic dinoflagellate Karenia brevis using gyroxanthin-based detection methods, J. Appl. Phycol., 16, 315–328, https://doi.org/10.1023/B:JAPH.0000047788.31312.4f, 2004.

Sal, S., López-Urrutia, Á., Irigoien, X., Harbour, D. S., and Harris, R. P.: Marine microplankton diversity database: Ecological Archives E094-149, Ecology, 94, 1658–1658, https://doi.org/10.1890/13-0236.1, 2013.

Sellner, K. G.: Plankton productivity and biomass in a tributary of the upper Chesapeake Bay. I. Importance of size-fractionated
335   phytoplankton productivity, biomass and species composition in carbon export, Estuar. Coast. Shelf Sci., 17, 197–206, https://doi.org/10.1016/0272-7714(83)90064-1, 1983.

Stauber, J. L. and Jeffrey, S. W.: Photosynthetic pigments in fifty-one species of marine diatoms, J. Phycol., 24, 158–172, https://doi.org/10.1111/j.1529-8817.1988.tb04230.x, 1988.

Stock, C. A., Dunne, J. P., and John, J. G.: Global-scale carbon and energy flows through the marine planktonic food web: An
340   analysis with a coupled physical–biological model, Prog. Oceanogr., 120, 1–28, https://doi.org/10.1016/j.pocean.2013.07.001, 2014.

Stock, C. A., Dunne, J. P., Fan, S., Ginoux, P., John, J., Krasting, J. P., Laufkötter, C., Paulot, F., and Zadeh, N.: Ocean Biogeochemistry in GFDL's Earth System Model 4.1 and Its Response to Increasing Atmospheric CO_2, J. Adv. Model. Earth Syst., 12, e2019MS002043, https://doi.org/10.1029/2019MS002043, 2020.

345   Ward, B. B.: Nutrients from CTD casts conducted on R/V Hugh R. Sharp cruise HRS2110 in the Chesapeake Bay during August 2021 (1), https://doi.org/10.26008/1912/bco-dmo.896158.1, 2023.

Wright, S. and Jeffrey, S.: Fucoxanthin pigment markers of marine phytoplankton analysed by HPLC and HPTLC, Mar. Ecol. Prog. Ser., 38, 259–266, https://doi.org/10.3354/meps038259, 1987.